CHAPTER 4

Result and Discussions

4.1 Plasma Source Ion implantation

The effect of the time period in the range of 0-30 μs of the electrical pulse, λ_0 (i.e., 0, 1.5, 3.0,15, and 30 μs) on the hydrogen ion density distribution in the plasma field was studied (figure 4.1-4.5). The results at 30 μs were chosen and normalized to compare each other. It was found that the results observed at 30 μs are varied; the ion density distributions are somewhat different. However, it is important to note that in the case of non negative biased system (λ_0 = 0 μs), the ion density distribution is significantly different as compared to the one with the electrical pulse. Figure 4.6a-4.6b showed the movement of hydrogen ions in plasma field under the highly negative voltage pulse biased in form of the time period in plasma source ion implantation system. Moreover, the frequency of ion movement was showed in those figures. From the periodic boundary condition, the Debye Shield effect did not significant and due to the over estimate of the ion flux.

To clarify how ion density distribution is changed through out the observation time, the ion flux density distribution that past through once area were plotted and shown in figure 4.7. When the given frequency is below to the plasma frequency the ion flux density increases with the increasing of the given frequency. In the other cases, the given frequency is higher than the plasma frequency; the ion flux density is constant. The results suggest that the effects of the electrical pulse with the given periods are similar

when the given frequency is higher than. For figure 4.8 showed the result of the ion energy and velocity when increases the bias potential with the fixed frequency. The increasing of the ion energy is proportional to the bias potential. Moreover the size of the ion affects the ion energy in the electric field. The smaller one has the higher ion velocity so that the ion energy is higher. The basic idea of the plasma source of the heavy ion implantation is to use the specific features of the ion interaction with matter. First of all, heavy ions have a very high energy loss in matter which scales quadratically with the charge of the projectile and allows high ion flux densities in the medium. Secondly, heavy ions have a unique ability to produce non-thermal excitation of atoms and molecules of the stopping medium. And finally, heavy projectiles have a small angular scattering in the propagated medium. For all of the above reasons, the study decides to use the heavy ions in the simulation. The energy profile of a Pt ion in figure 4.9 showed the ion movement started from the chamber boundary then traveled through the plasma field and ended at the target material. The ion energy was increased by the negative high voltage bias.

λ_0 is 30 μs

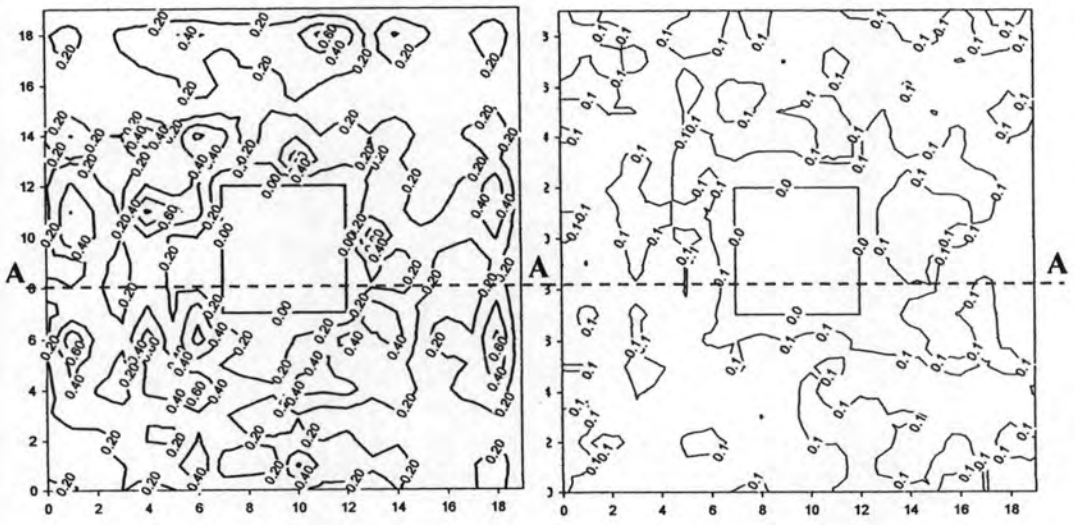

Fig. 4.1A normalized ion density at 8 cm. height of 30 μs time

Fig. 4.1B normalized ion density at 8 cm. height of staring time

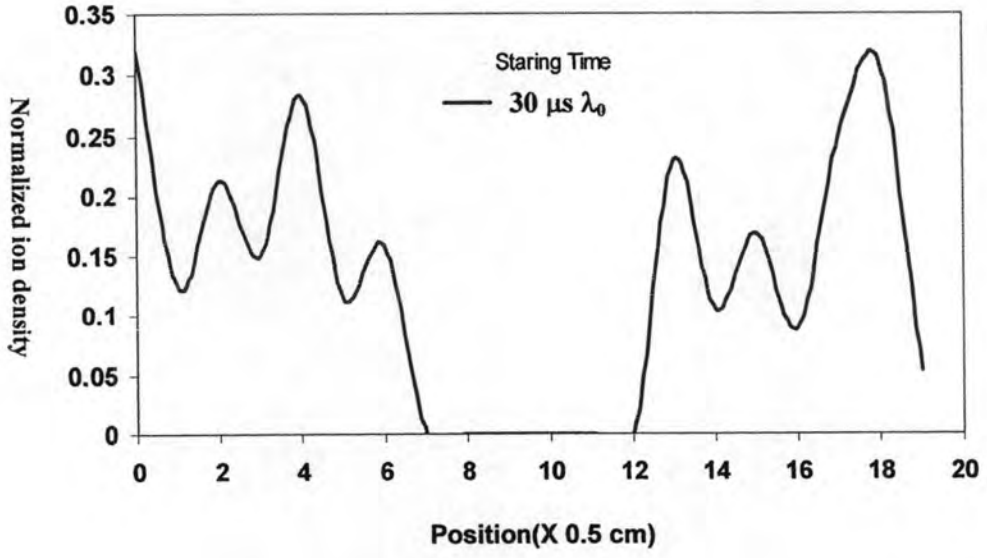

Fig. 4.1C normalized ion density at section AA

Fig. 4.1 The relationship of normalized ion density at 30 μs λ_0

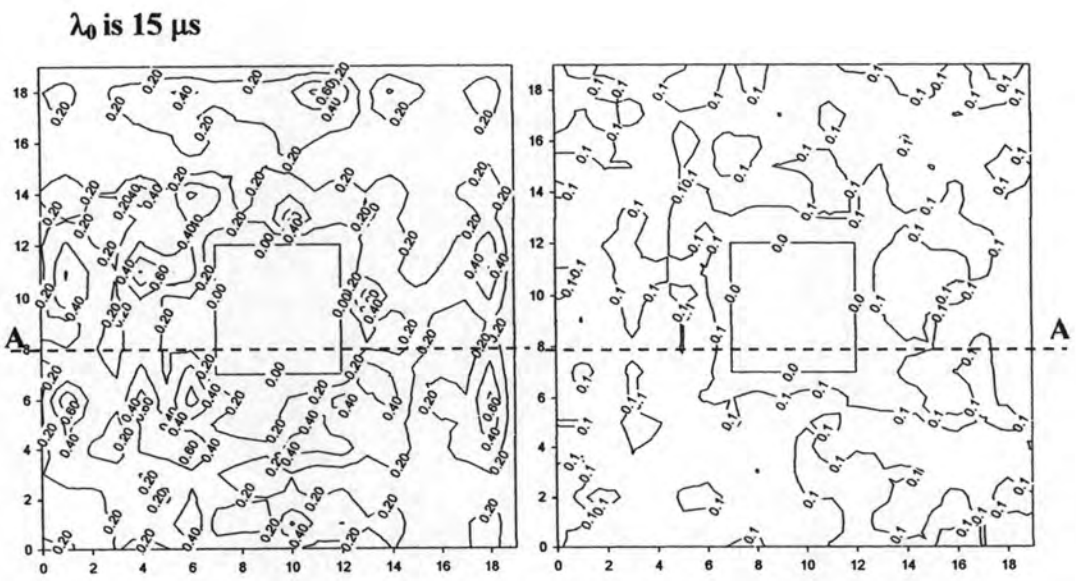

Fig. 4.2A normalized ion density ats8 cm. height of 30 μs time

Fig. 4.2B normalized ion density at 8 cm. height of staring time

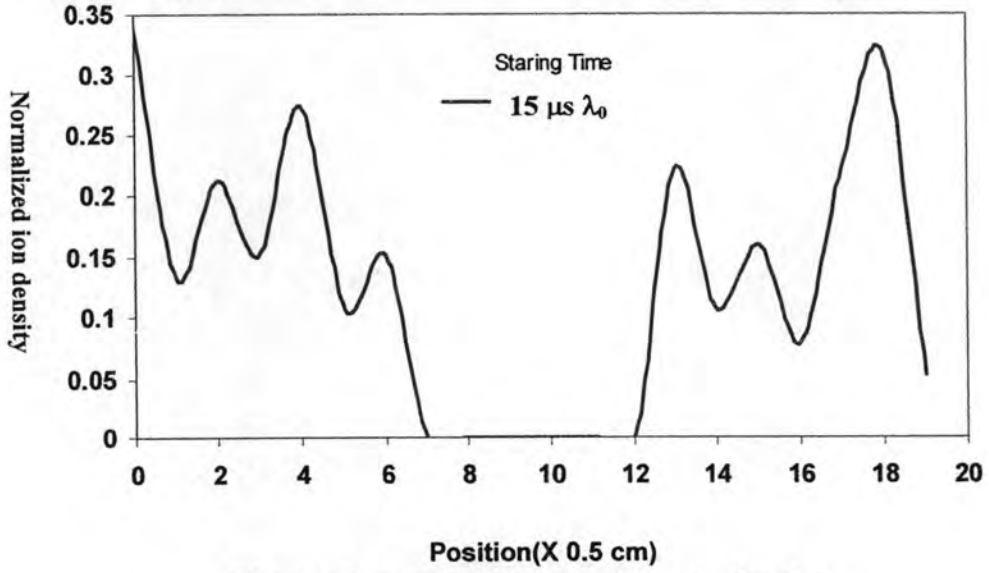

Fig. 4.2C normalized ion density at section AA

Fig. 4.2 The relationship between normalized ion densities at 15 μs λ_0

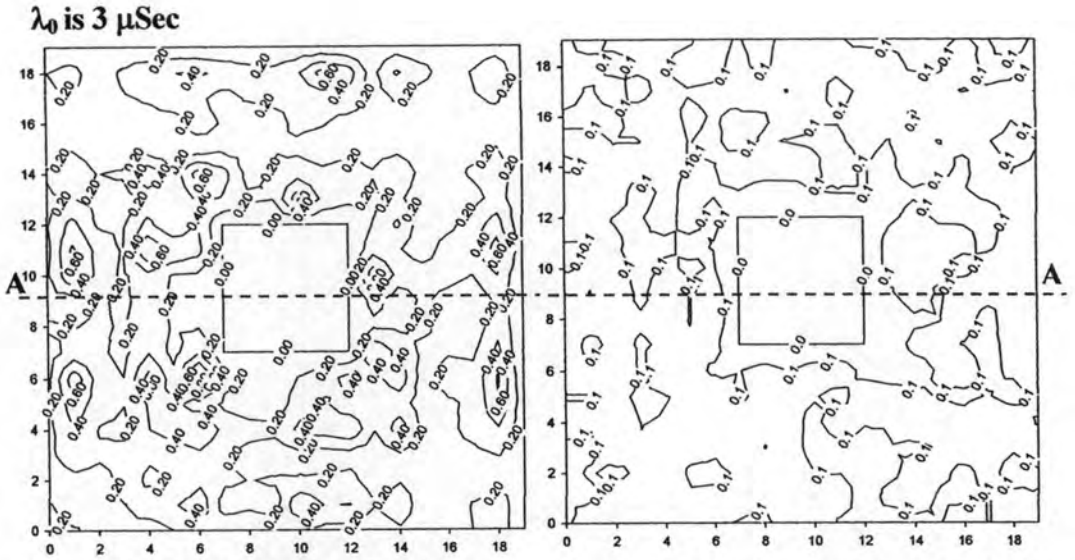

Fig. 4.3A normalized ion density at 8 cm. height of 30 μs time

Fig. 4.3B normalized ion density at 8 cm. height of staring time

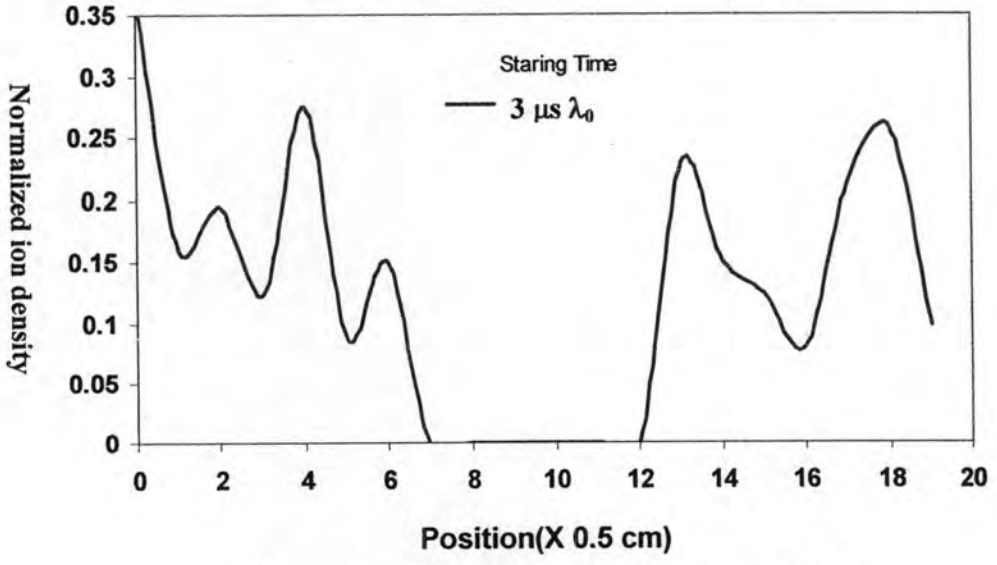

Fig. 4.3C normalized ion density at section AA

Fig. 4.3 The relationship of normalized ion density at 3 μs λ_0

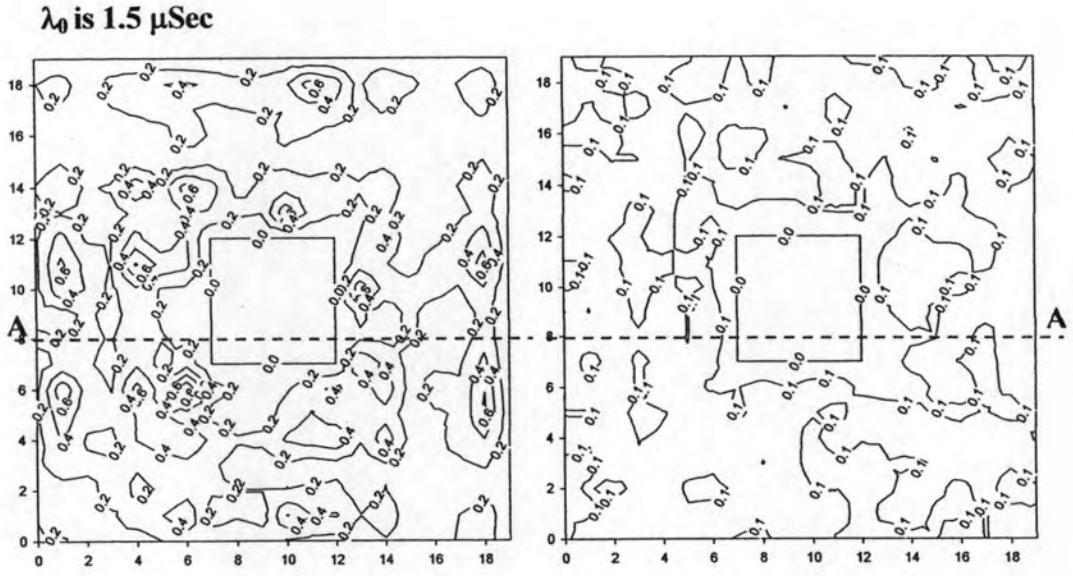

Fig. 4.4A normalized ion density at 8 cm. height of 30 μs time

Fig. 4.4B normalized ion density at 8 cm. height of staring time

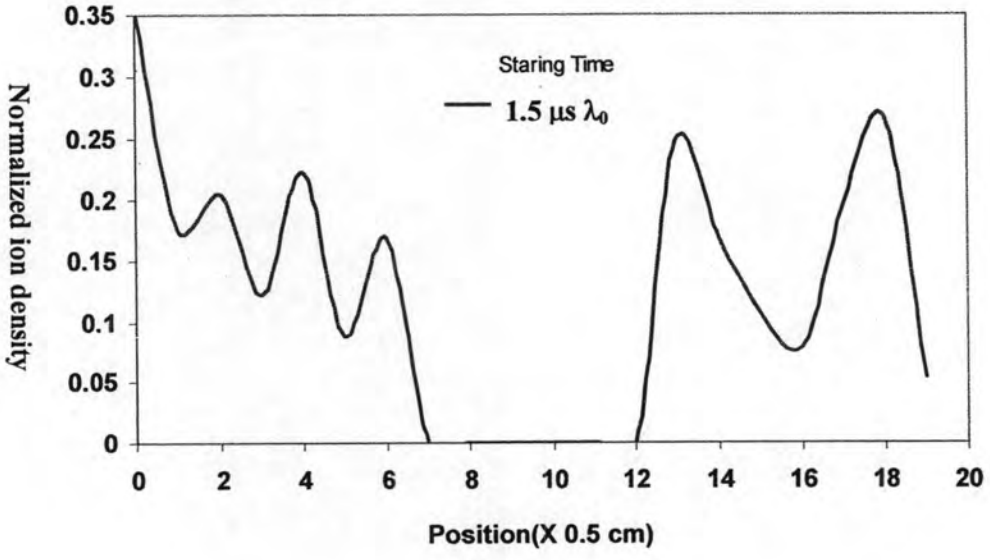

Fig. 4.4C normalized ion density at section AA

Fig. 4.4The relationship of normalized ion density at 1.5 μs λ_0

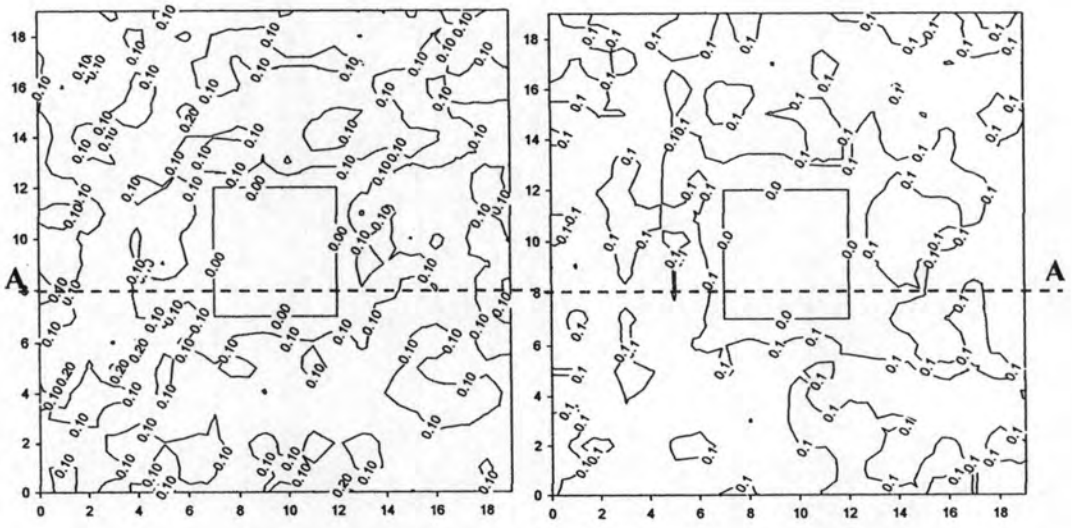

Fig. 4.5A normalized ion density at 8 cm. height of 30 μs time

Fig. 4.5B normalized ion density at 8 cm. height of staring time

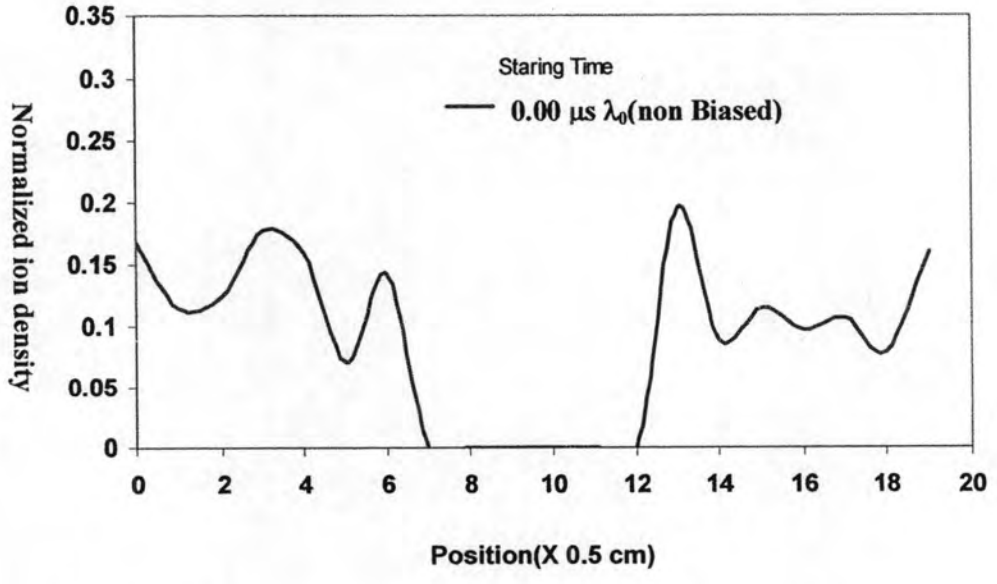

Fig. 4.5C normalized ion density at section AA

Fig. 4.5 The relationship of normalized ion density at 0 μs λ_0 (non biased)

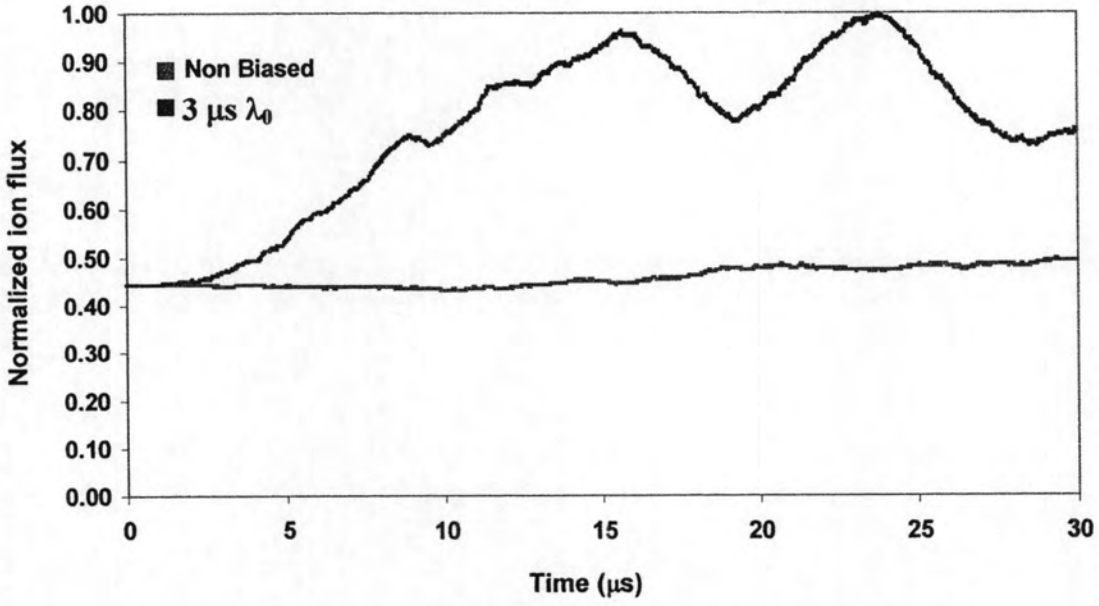

Fig. 4.6a The effect of negative high voltage pulse biased time period that is 3 μs in plasma flux movement

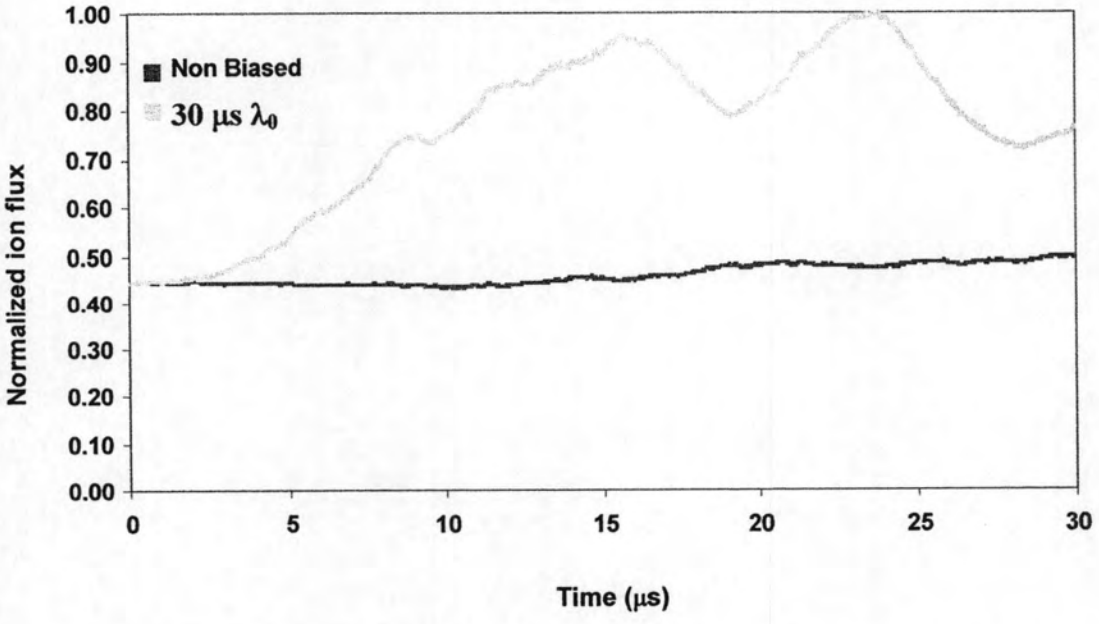

Fig. 4.6b The effect of negative high voltage pulse biased time period that is 30 μs in plasma flux movement

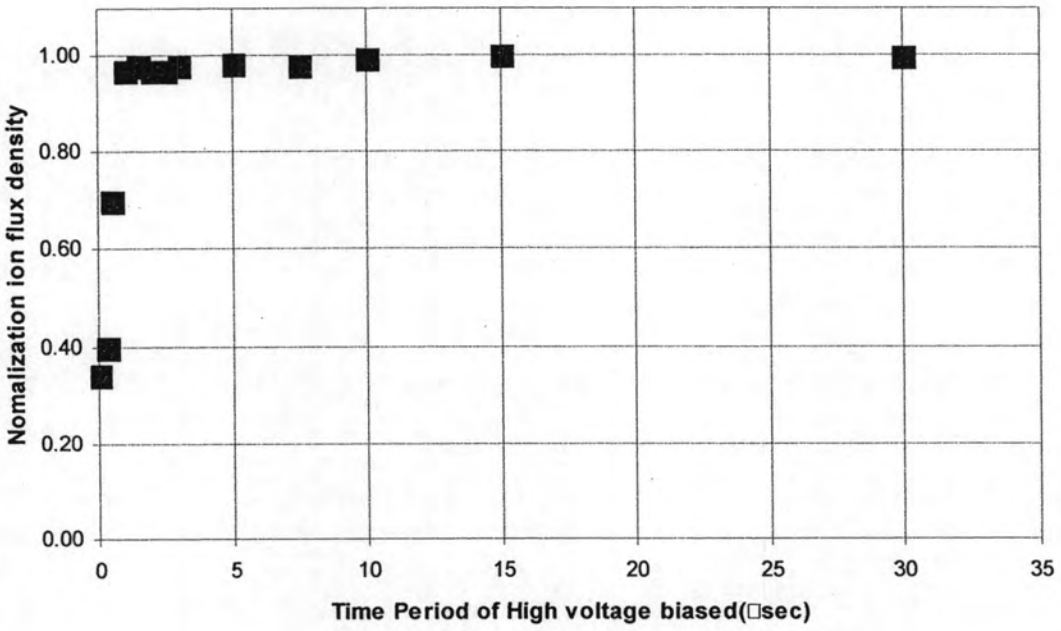

Fig. 4.7a The relationship of normalized ion flux density and time period

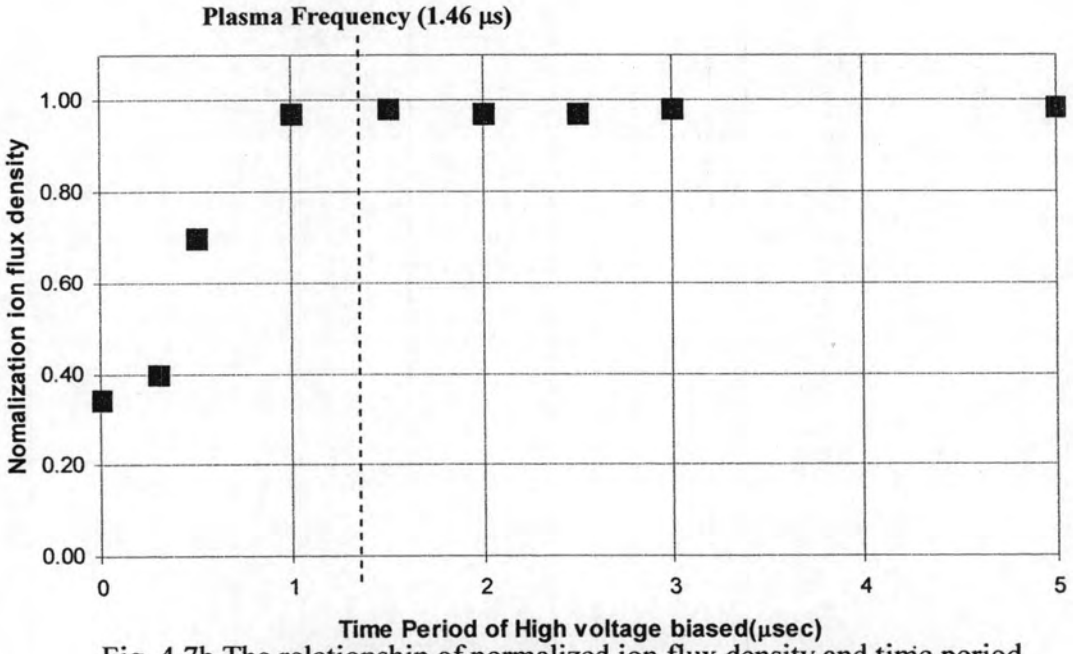

Fig. 4.7b The relationship of normalized ion flux density and time period

Fig. 4.7 The relationship of normalized ion flux density and time period

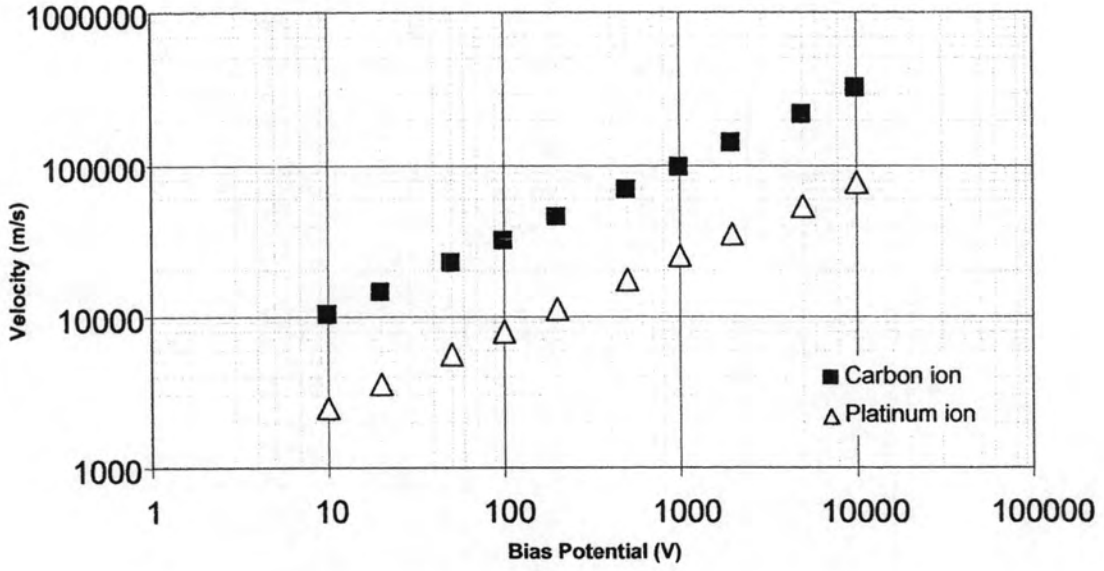

Fig. 4.8a The relationship of ion velocity and bias potential

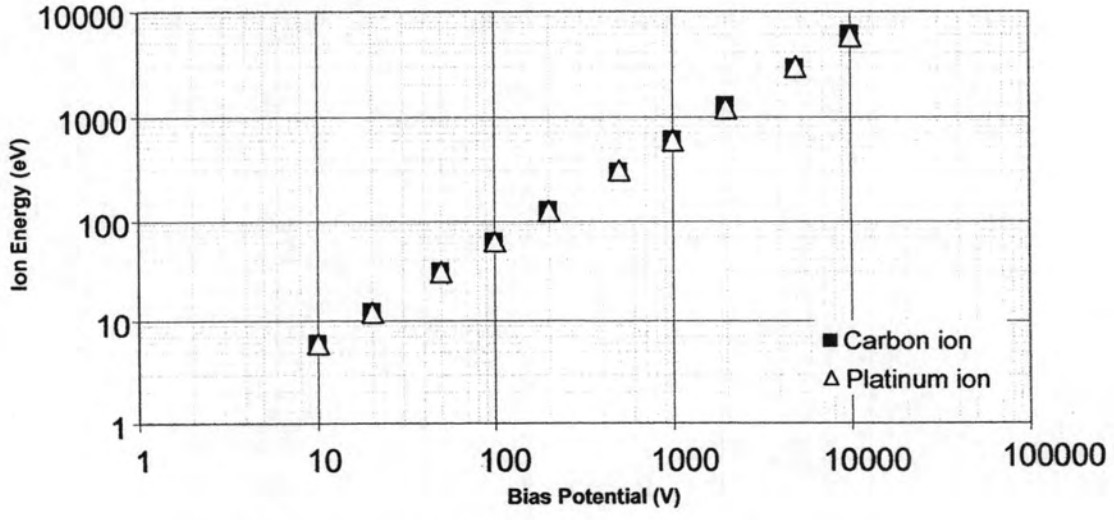

Fig. 4.8b The relationship of ion energy and bias potential

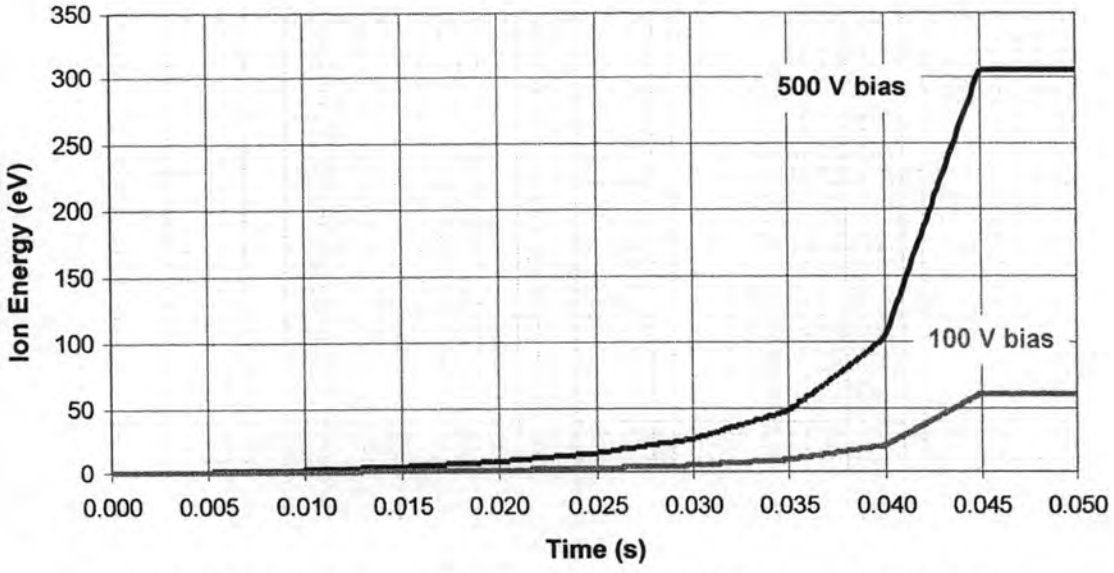

Fig. 4.9 The relationship of the increasing of the ion energy with time

4.2 Ion Implantation

From the simulation, the types of the ion pathways in the implantation process were classified as three types. Fist type was due to the scattering effect. The ion with this type could not penetrate into the crystalline medium. The second type, the implantation type which the ion penetrated through the medium and implanted in, was shown in Figure4.10a. For the other type of the crystalline medium likes BCC, the ion trajectory for the implantation type seemed to be similar as shown in Figure 4.11. The last type of path way was caused by the channeling effect and shown in Figure4.10b. For this pathway, an ion traveled through the open channel in the lattice with the stopping inside so that the implantation did not occur. The percent of each path way types showed in Table 4.2. With different initial energy of ions, the number of ions happened those three path ways were different. For low energy ions, the percent of the scattering increased. On the other hand, the percent of the channeling and the implantation increased with high

energy ions. In the table indicated that the probability of the channeling was too low until met the high energy ions, 2000 MeV.

Table 4.1 the physical constants of the basement material with Z = 26 and the coating atom with Z = 78

Element	Z	Mass (amu.)	σ (eV)	ε (A)	σ_{Fe-Pt} (eV)	ε_{Fe-Pt} (A)
Basement material with Z = 26	26	55.845	3.496(BCC) 3.856 (SC)	2.554(BCC) 2.209 (SC)	3.1040* 3.2599**	2.988* 2.779**
Coating ion with Z = 78	78	195.078	2.756(FCC)	3.496(FCC)		

** Fe Lattices structure is BCC (Body Center Cubic)*
*** Fe Lattices structure is SC (Simple Cubic)*

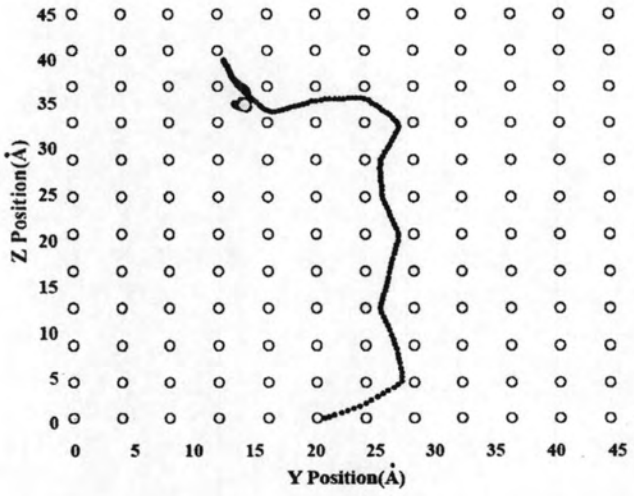

Fig. 4.10a The track of the 800eV coating ion with Z = 78 implanted in the simple cubic basement material with Z = 26

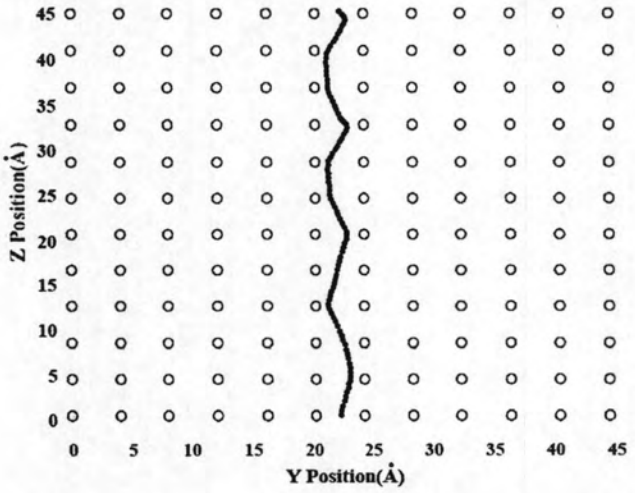

Fig. 4.10b The channeling effect on the track of the 800eV coating ion with Z = 78 in the simple cubic basement material with Z = 26

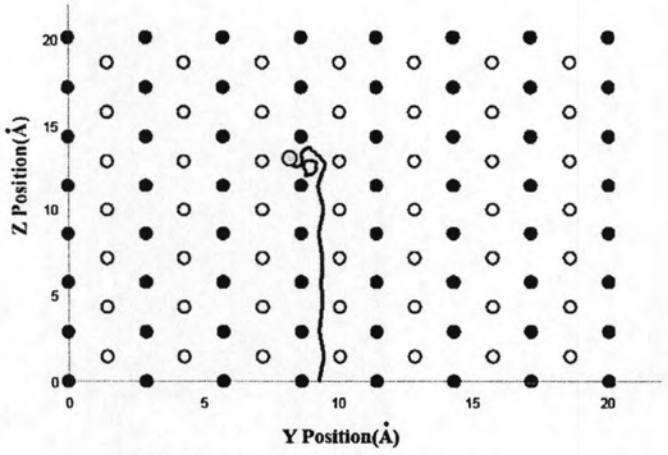

Fig. 4.11 The track of the 800eV coating ion with Z = 78 implanted in the BCC basement material with Z = 26

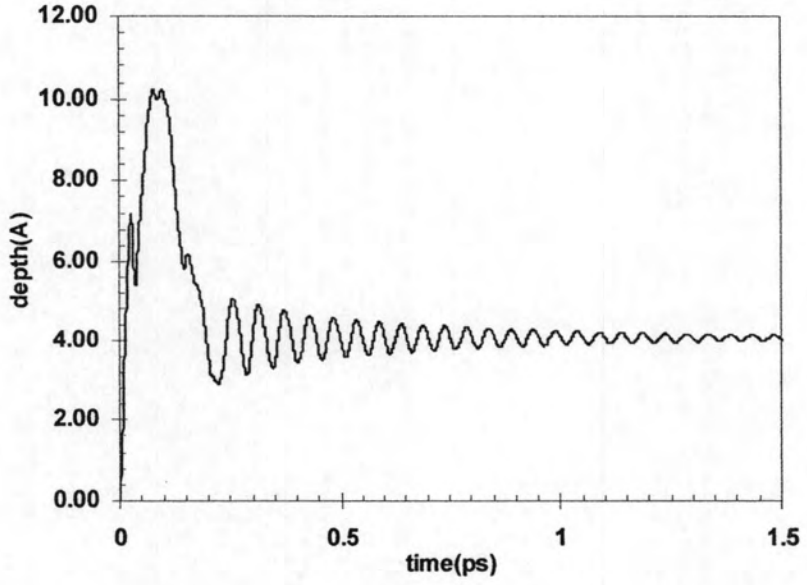

Fig. 4.12 Movement on Z axis of the 200eV coating ion with Z = 78 implanted in the SC basement material with Z = 26

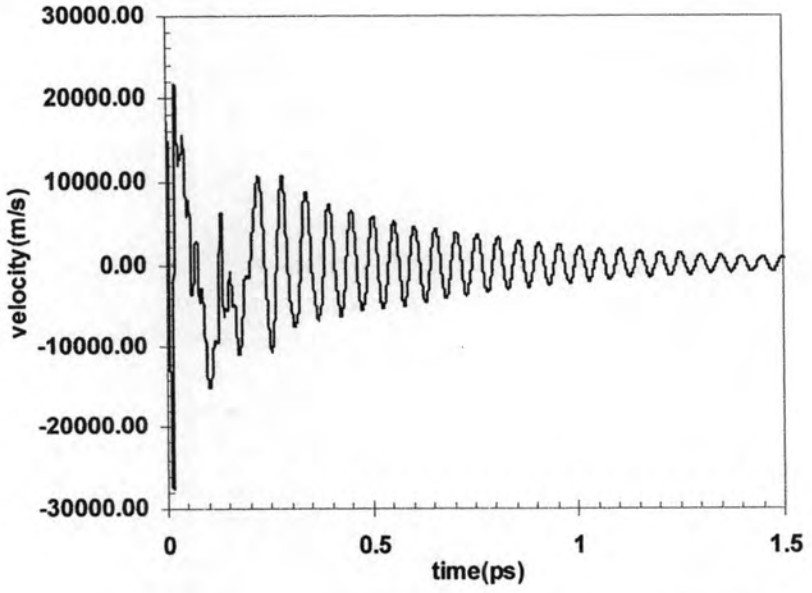

Fig. 4.13 Velocity profile of the 200eV coating ion with Z = 78 implanted in the SC basement material with Z = 26

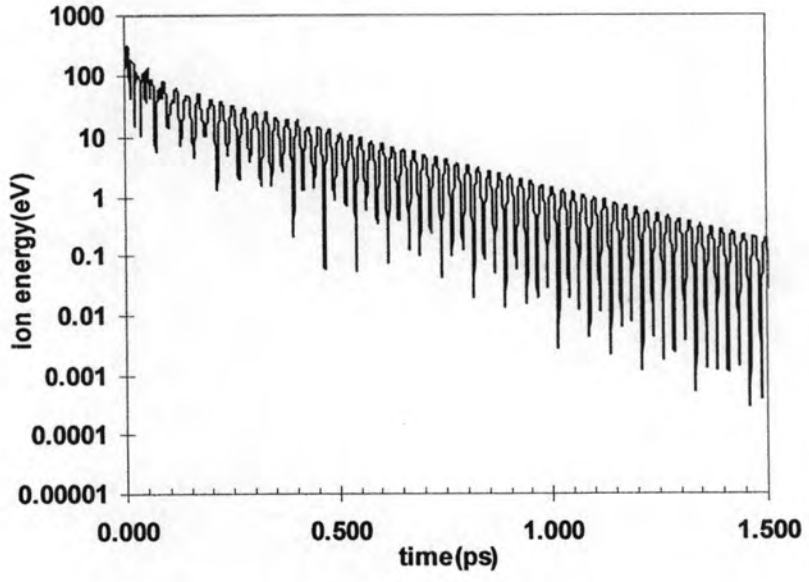

Fig. 4.14 The energy profile of the 200eV coating ion with Z = 78 implanted in the SC basement material with Z = 26

Table 4.2 % of each path ways at different ion energies

Energy(eV)	%Scattering	%Channelling	%Implantation
125	50.7753877	1.70085043	47.5237619
300	38.7693847	2.4012006	58.8294147
500	39.1695848	4.30215108	56.5282641
2000	20.2101051	42.4212106	37.3686843

The energy profile of an ion implantation in the crystalline medium showed in figure 4.14. The ion energy gradually reduced with time. The simulation presented the present of ion frequency for the implantation process. There were few number of ions penetrated through the longer depth of the crystalline medium. So that in figure 4.15a-4.15c at the longer depth showed the lower ion frequency. When increased the ion energy, the ion frequency at the longer dept had increased moreover the ion distribution was increased and smoother.

In the simulation of BCC medium, the profile of the ion frequency was similar with the first simulation, SC but there was a very high ion frequency at the short depth. Figure 4.16a – 4.16c described the ion frequency in the BCC medium at the various ion energies.

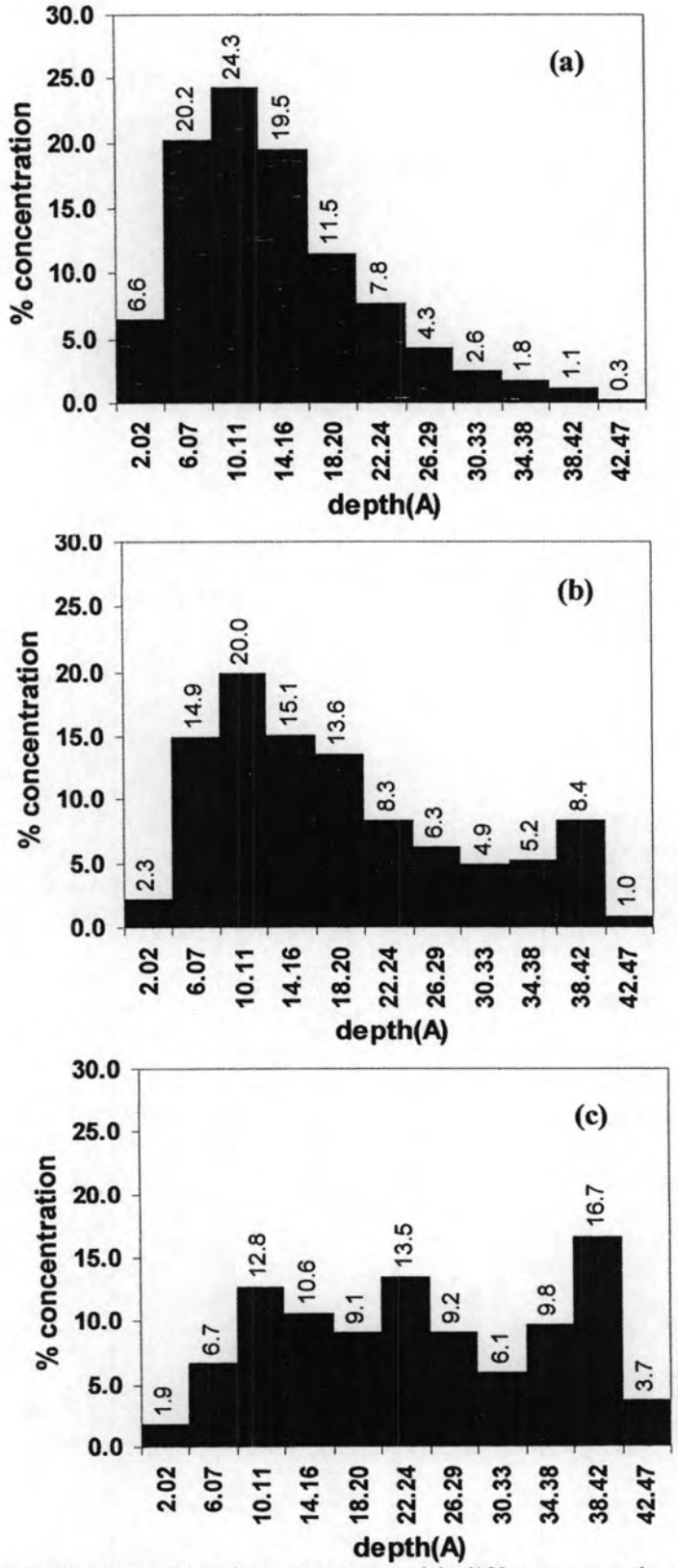

Fig. 4.15 Distribution of the ions (Z = 78) with different energies: (a) 200 eV, (b) 600 eV, and (c) 1000eV implanted on the SC lattice basement material (Z = 26).

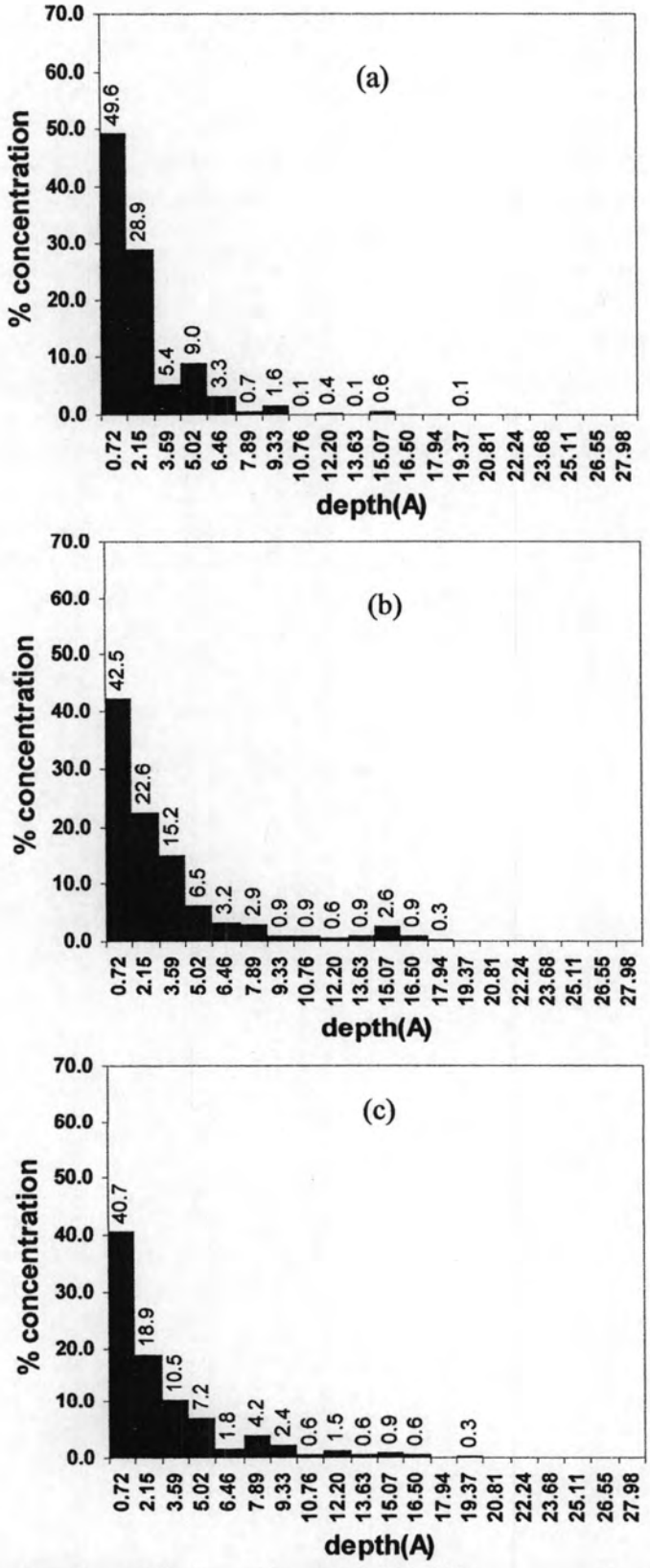

Fig. 4.16 The distribution of the ions (Z = 78) with different energies: (a) 200 eV, (b) 600 eV, and (c) 1000eV implanted on the BCC lattice basement material (Z = 26).

In general, the average range of the ion in the medium depended directly with the initial energy of the ions. The simulation result of the average range of the ions at the different ion energy was shown in figure 4.19. Moreover the study compared the results with the ion range calculated with TRIM/SRIM in that figure. Those 3 results from MD (SC), MD (BCC) and TRIM/SRIM had the similar trend on the effect of the initial energy of the ion. In that way, the TRIM/SRIM result had medium value of the ion range between those two results from MD. The study had simulated the implantation of the natural crystalline medium, 5MeV He ions in Ta and gave the similar result with the previous one as shown in figure 4.18. The highest amount of 5 keV He ions in BCC Ta target was 58 % at the range of 75 A and it was gradually decreased as the depth of interest was increased. The range calculated by the molecular dynamic simulation and the standard TRIM/SRIM model were 128.246 and 131 A respectively. The experimental result of J. R. Conrad [4] showed the distribution of N^+ ions implanted in the Si crystalline medium in figure 4.19. The simulation result of molecular dynamic of N^+ ions implanted in the Si crystalline medium was compared in that figure. From the comparison, those of experimental and simulation results showed the similarly trend of ions distribution, thus there were some different from the original direction of ions. In the experiment, the ions had a several direction to implant in the medium whereas; the simulation ions were fixed direction to perpendicular with crystal plane. The average ranges were similar and result were 331.2893, 370.1077, 330.000 A gotten from the molecular dynamic simulation, the experimental and TRIM/SRIM respectively.

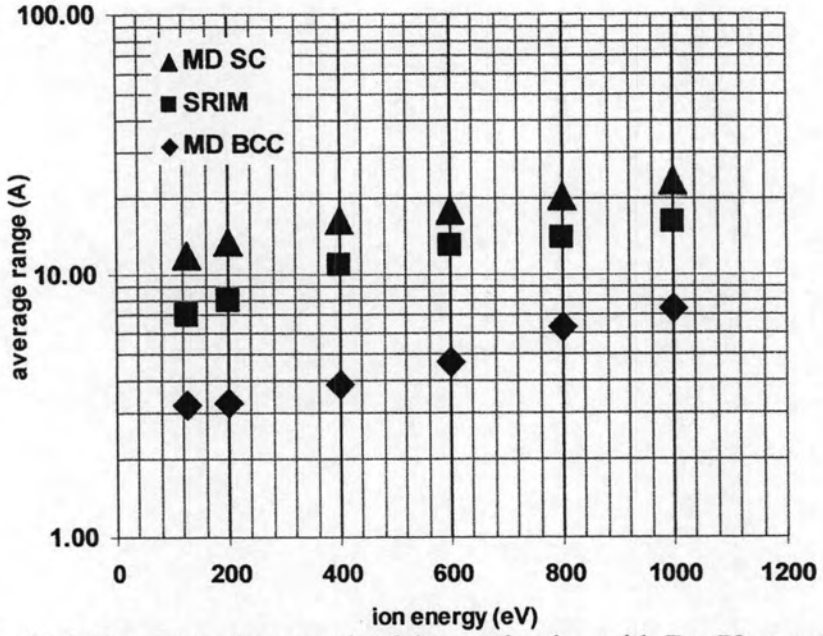

Fig. 4.17 The comparison result of the coating ion with Z = 78 range in the basement material with Z = 26 by difference methods and structures

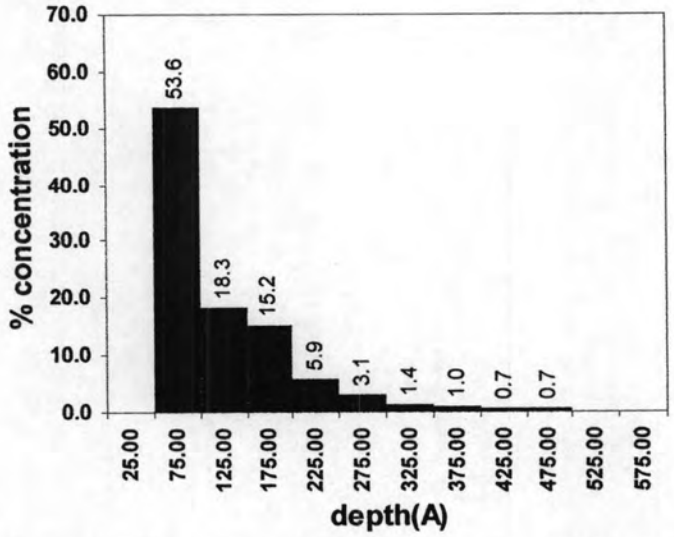

Fig. 4.18 The distribution of 5 keV He ions implanted in the BCC Ta

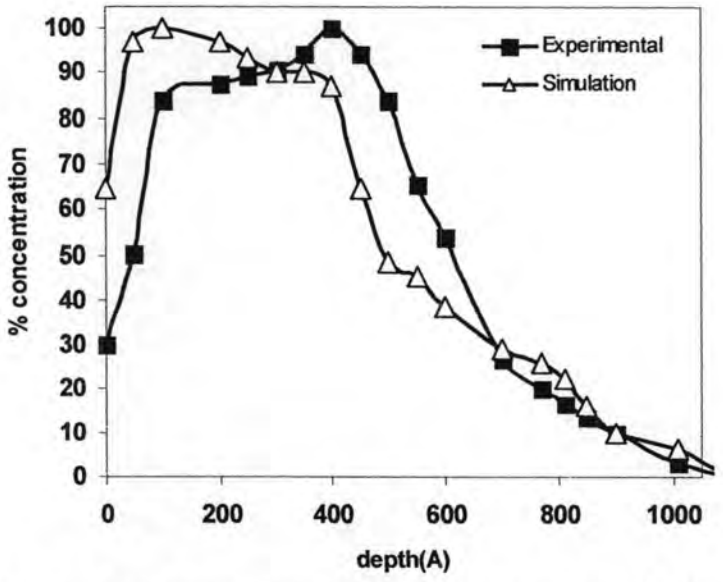

Fig. 4.19 The distribution of 25 keV N^+ ions implanted in the Si crystalline structure

4.3 Ion Coating

From the simulation, the model of the coating process was proposed. The track of the first ion movement was show in figure 4.20. The ion distance increased with time and then the distance would constant at the certain time. That figure showed the ion range got from the several values of ***K***. Some values of ***K*** give the deviation in the ion range from SRIM/TRIM. In the simulation with ***K*** = 6.875 unit, the ion had the deepest distance resembled with the ion range calculated by SRIM/TRIM. The comparison of 3^{rd}, 7^{th}, 29^{th}, 30^{th} and 50^{th} ion movement was shown in figure 4.23 presented the same process with the first one but in the shorter length. The ion velocity and the ion energy at different times were presented in figure 4.21 and figure 4.22 respectively. Those figures shown the same relation, the velocity and the energy of the ion were reduced by time that ion traveled

through the target material. The result of the total interaction in the coating process was presented in the schematic of the coating of the ion on the crystalline target, figure 4.24.

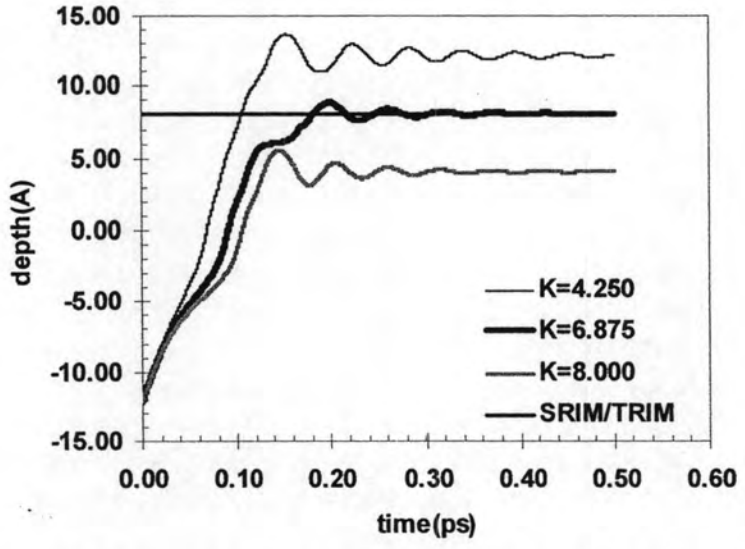

Fig. 4.20 The movement on Z axis of the first 200eV coating ion with Z = 78 implanted on the SC target with Z = 26

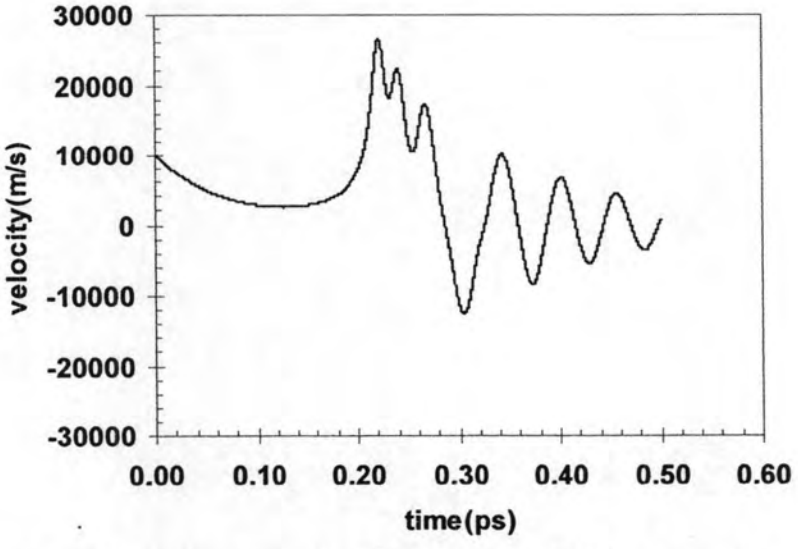

Fig. 4.21 The velocity on Z axis of the first 100eV coating ion with Z = 78 implanted in the SC target with Z = 26

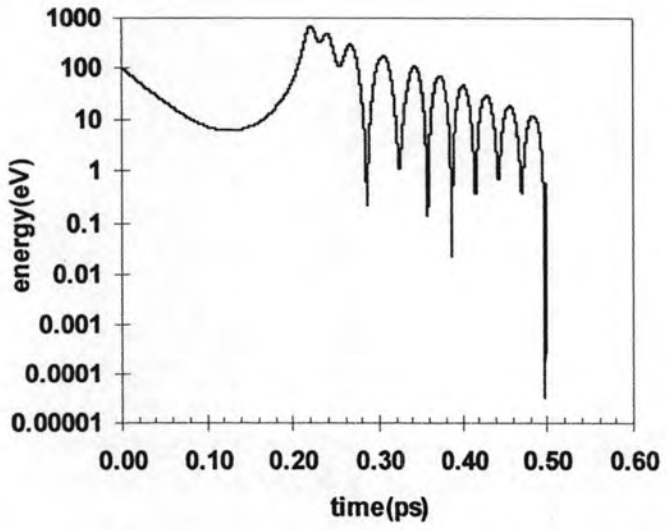

Fig. 4.22 The energy profile of the first 100eV coating ion with Z = 78 implanted in the SC target with Z = 26

The process created the mix layer zone in the crystalline medium that had the maximum depth equaled with the ion range. The study estimated the time created the mix layer zone as shown in table 4.3. Moreover, the properties of the mix layer zone, the range of mix layer zone, the radius and the ion density in mix layer zone were proposed by the study. The time results showed in the table were the average value from the times of each crystalline column in the simulated mix layer zone, a crystalline column defined as the crystalline medium volume with the 1 unit cell width, 1 unit cell length and the ion range depth.

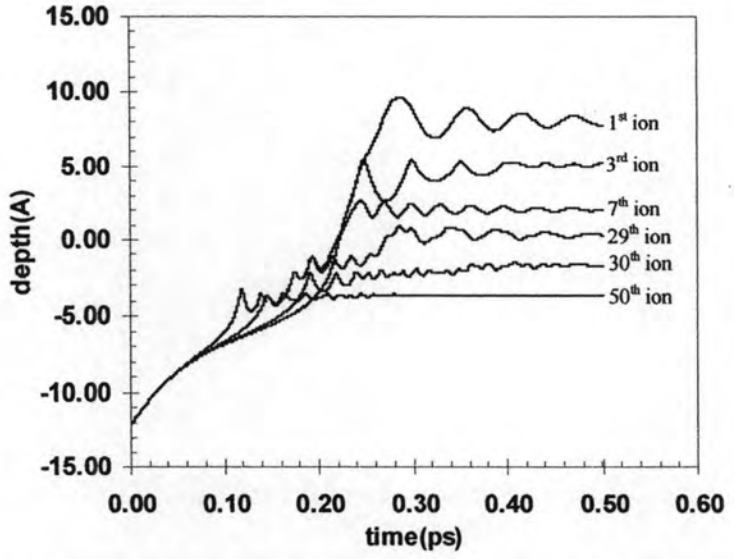

Fig. 4.23 The movement on Z axis of the first 200eV coating ion with Z = 78 implanted in the SC target with Z = 26

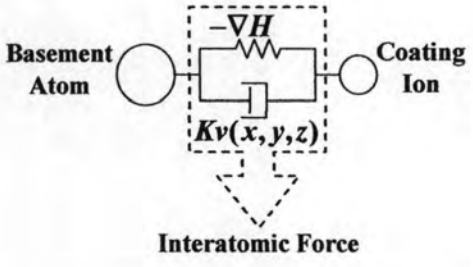

Fig. 4.24 Schematic of two body interatomic force equivalent between implanted ion and basement atom

The following figure, figure 4.25 indicates that the higher energy ion (800eV) penetrates into the medium with the higher ion range than the lower energy ion (200eV). When considering in the ion energy, the ion with the lower energy take the shorter time to meet the equilibrium as see in figure 4.26a-b. The time that ion met the equilibrium point counts from the started time to the time that the ion energy remains 10% of the initial energy. Figure 4.26b showed the equilibrium time taken by the ion, the higher

energy ion has the higher equilibrium time. From figure 4.27, it shows the equilibrium position that the ion energy remains 10%

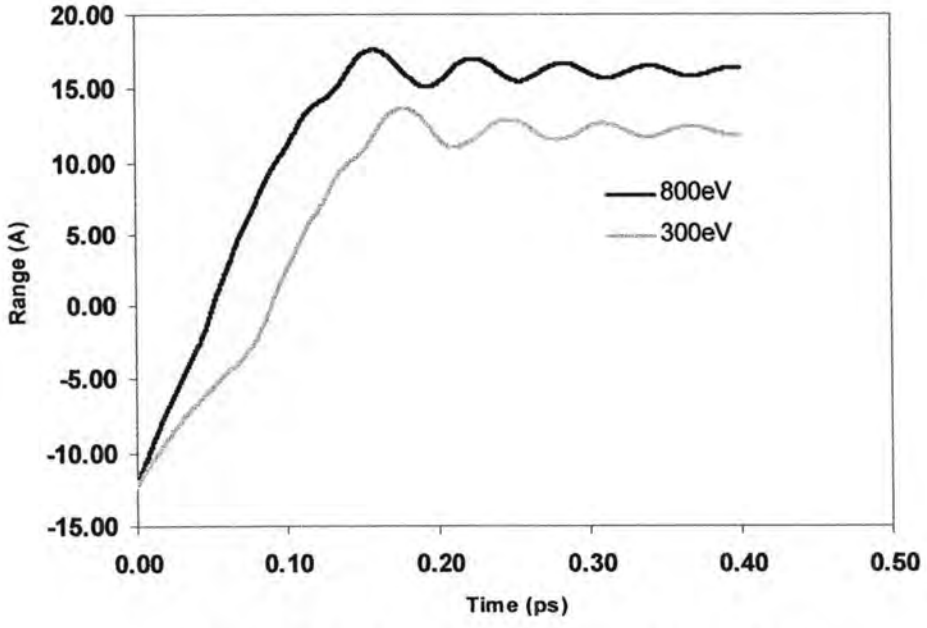

Fig. 4.25 The trajectory profile of the first coating ion with Z = 78 implanted in the SC target with Z = 26

When the coating ions from the PSII bombarded to the crystalline medium, the interaction between the ion and the medium matter had effected to the pathway type. The ions with the scattering effect scatted out of the medium surface so that those ions could not pass through the medium. Initially an ion would travel in a straight direction beginning from the point of scattering or the point of its origination. In a presence of an electromagnetic field, an ion could be accelerated and deviated from its original direction. At each scattering, however, the ion could abruptly change the direction. For this process, it was assumed that the scattering is isotropic. The other ions traveled through the crystalline target, their kinetic energy were reduced due to the interatomic force exerted by the medium lattices as defined by LJ potential and Universal ZBL potential. The

direction of the ion movement was also manipulated by both of potentials. After the certain time, the implantation occurred in the target because of the reducing of ion energy to zero or nearby. This interaction caused to the implantation pathway. The last type of path way was due to the channeling effect. For this pathway, an ion traveled for a long distance through the open channel in the lattice. The ion could not be effectively stopped by the interatomic potential and, therefore, can penetrate deeper than usual in to the medium.

As the defined layers (figure 4.28 and figure 4.29), the concentration at each layer or depth was different. The ions distributions at difference depths were shown in figure 4.33 – 4.35. The highest ion concentration located at the target surface and lower in the region inside and outside the target surface that belonged to the mixed layer and the coating layer respectively. Figure 4.35a-4.35c showed the ion distribution with the different random position incident. Both figures had a similar trend of the ion distribution.

From figure 4.30 – 4.32, they show track and position of coating ions (100eV, 200eV and 300eV) in XY plane and XZ plane.

Since the calculations are the periodic boundary condition, the coating patterns are same and repeat with every boundary in the medium as show in figure 4.29.

Table 4.3 the properties of the mix layer zone

Energy (eV)	Time (picoseconds)	Range of mix layer zone (A)	Ion density in mix layer zone(ion/m^3)
100	1.5953	4.0947	8.36229E+28
200	1.7469	7.9043	1.36481E+29
300	1.9185	13.5119	2.98268E+30

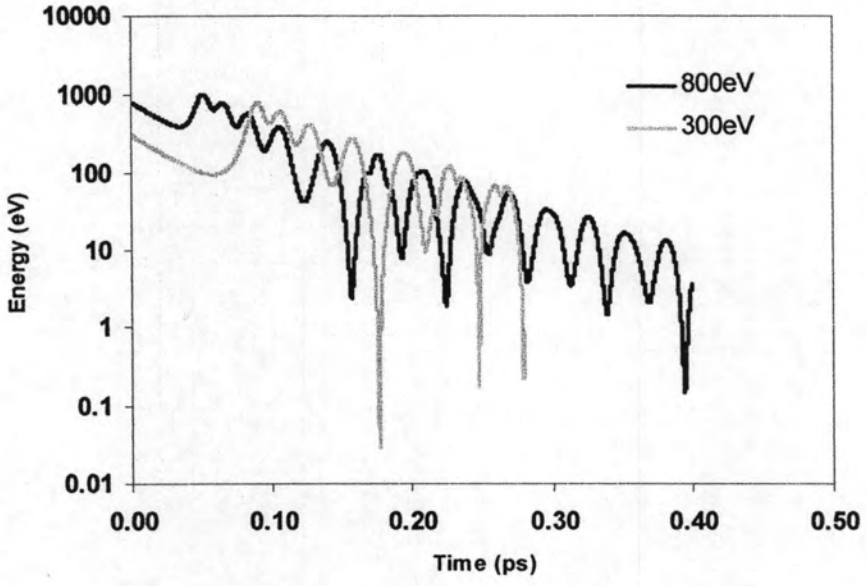

Fig. 4.26a The energy profile of the first coating ion with Z = 78 implanted in the SC target with Z = 26

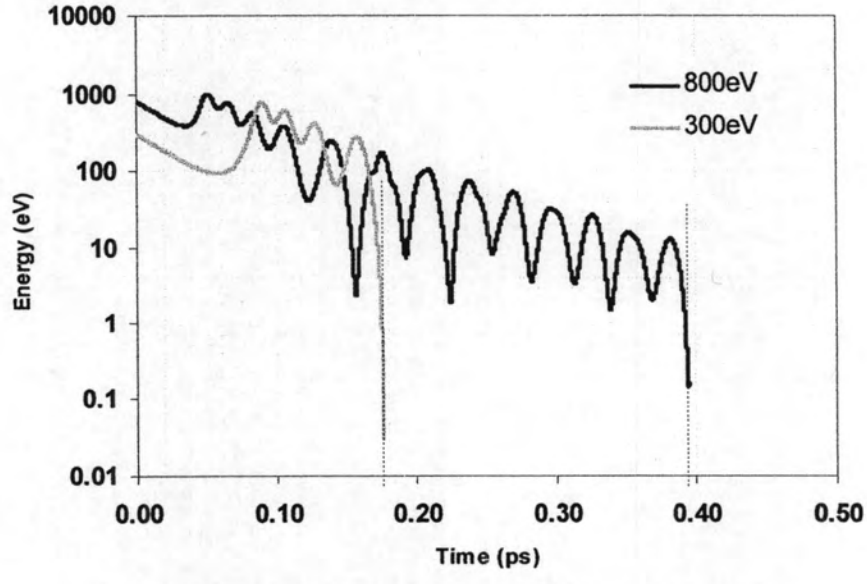

Fig. 4.26b The energy profile of the first coating ion with Z = 78 implanted in the SC target with Z = 26

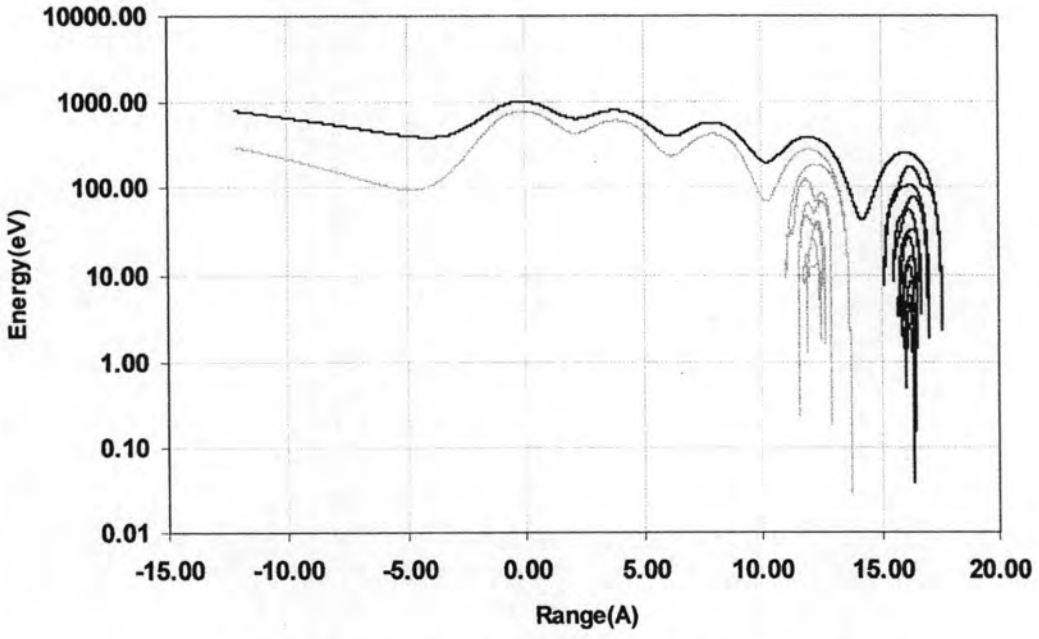

Fig. 4.27 The energy profile of Pt ion at different range

In this study, the simulation assumed that the coating ions with Z = 78 perpendicular traveled into the <100> plan of the crystalline target with Z = 26. When the later ions did not penetrate into the target, the coating process over the target had been occurred. The ion distribution at each region of the coating material was difference due to the effect of the interatomic force. From the equation 3.122-3.124, the later ions could not penetrate into the target as deep as the previous one. So that the more number of ions were trapped at the upper region above the ion range and caused the higher concentration. After the ion coated covered the entire substance surface, the coating ions at the surface acted like a new layer with the highest ion concentration. The next ions difficultly traveled through this layer. Thereby the ion concentration was decreased at the coating

depth increased. As the definition of the layers in the coating material above, there was not the ion concentration in the basement layer.

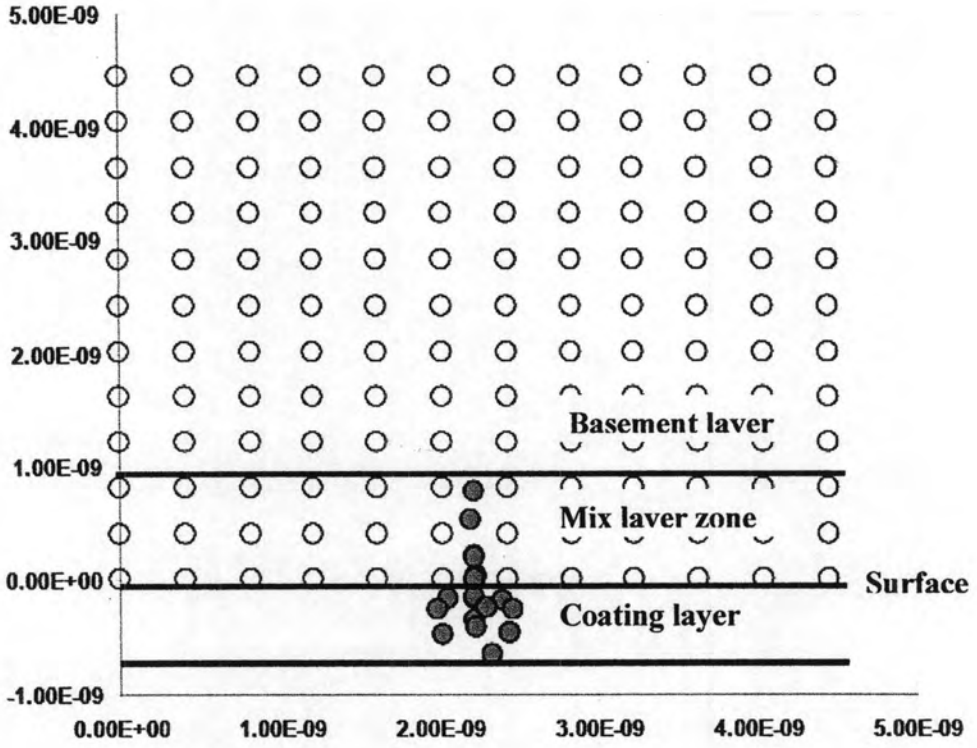

Fig. 4.28 The track of the 200eV coating ions with Z = 78 accumulate implanted in the SC target with Z = 26

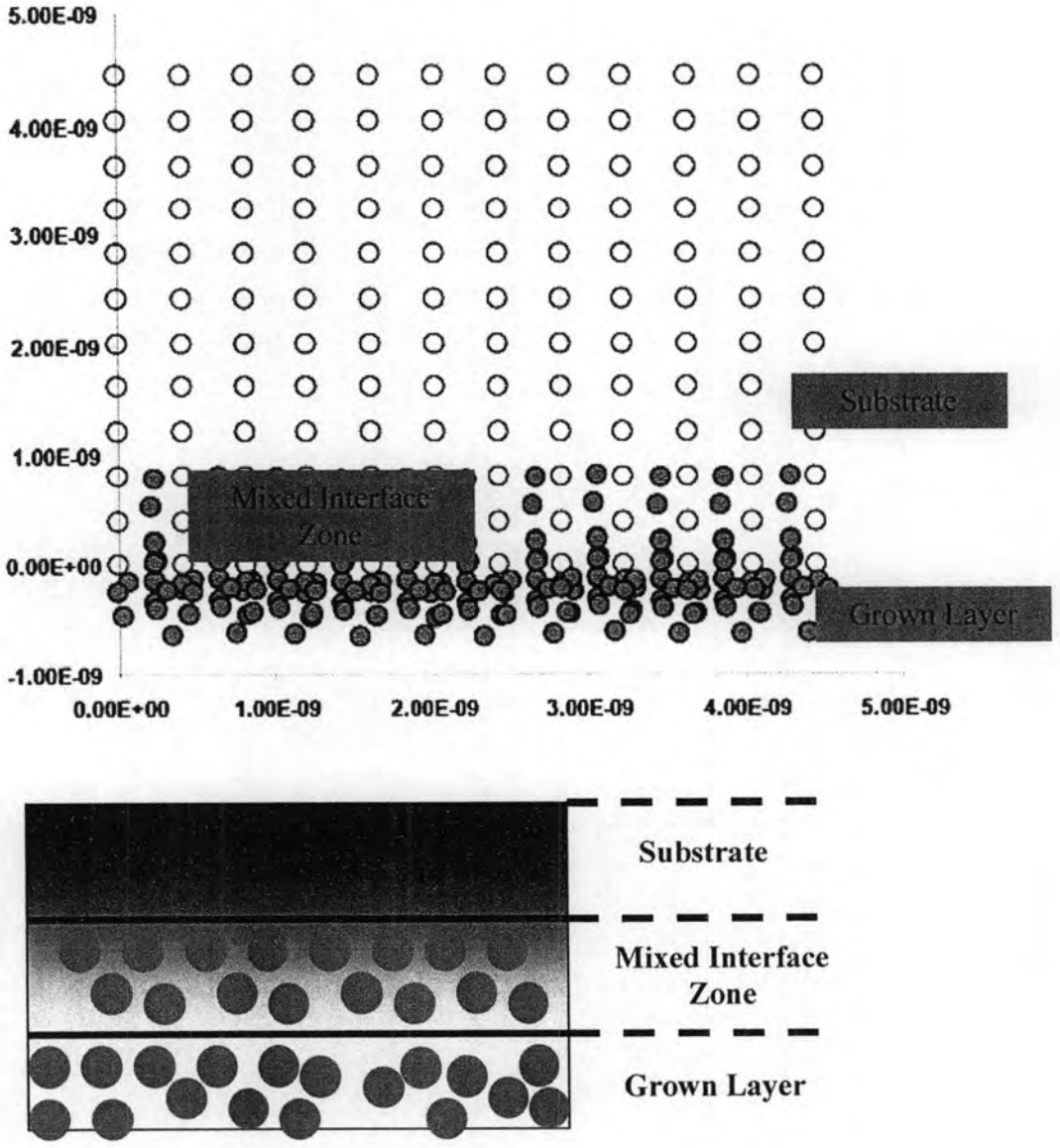

Fig. 4.29 The track of the 200eV coating ions with Z = 78 accumulate implanted in the SC target with Z = 26 that influence of periodic boundary condition

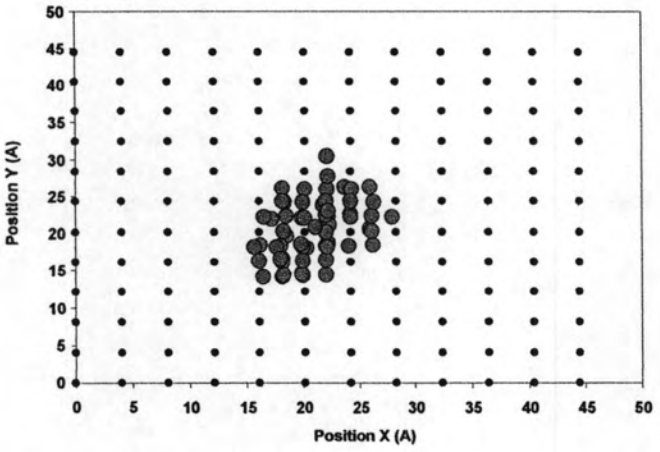

Fig. 4.30a The track of the 100eV coating ions with Z = 78 accumulate implanted in the SC target with Z = 26(XY Plane)

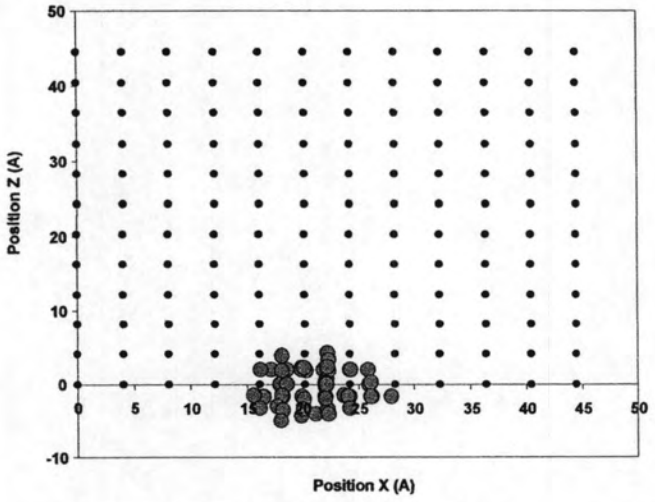

Fig. 4.30b The track of the 100eV coating ions with Z = 78 accumulate implanted in the SC target with Z = 26(YZ Plane)

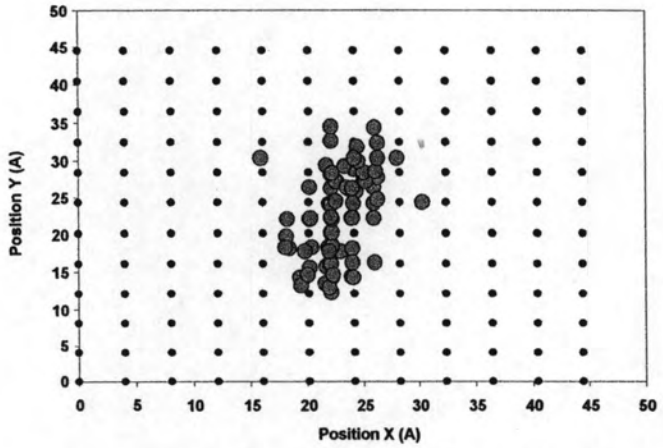

Fig. 4.31a The track of the 200eV coating ions with Z = 78 accumulate implanted in the SC target with Z = 26(XY Plane)

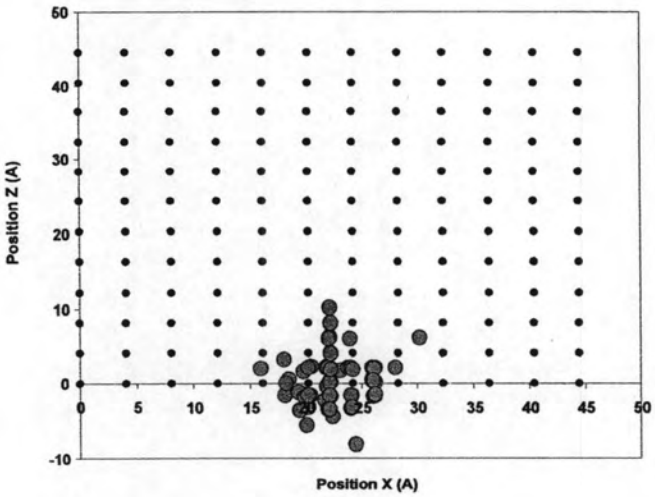

Fig. 4.31b The track of the 200eV coating ions with Z = 78 accumulate implanted in the SC target with Z = 26(YZ Plane)

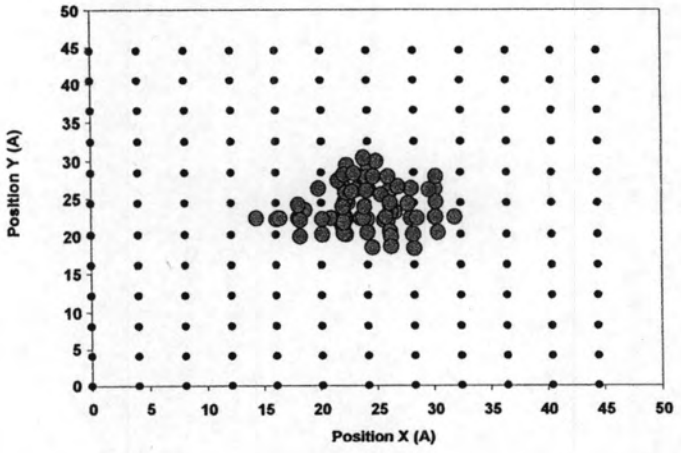

Fig. 4.32a The track of the 300eV coating ions with Z = 78 accumulate implanted in the SC target with Z = 26 (XY Plane)

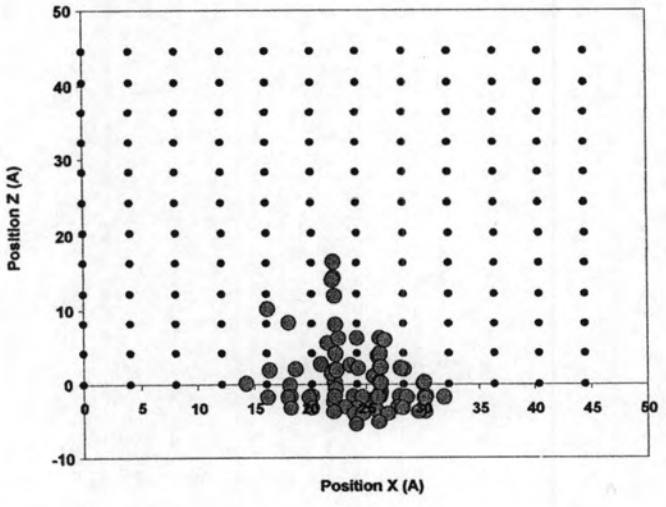

Fig. 4.32b The track of the 300eV coating ions with Z = 78 accumulate implanted in the SC target with Z = 26(YZ Plane)

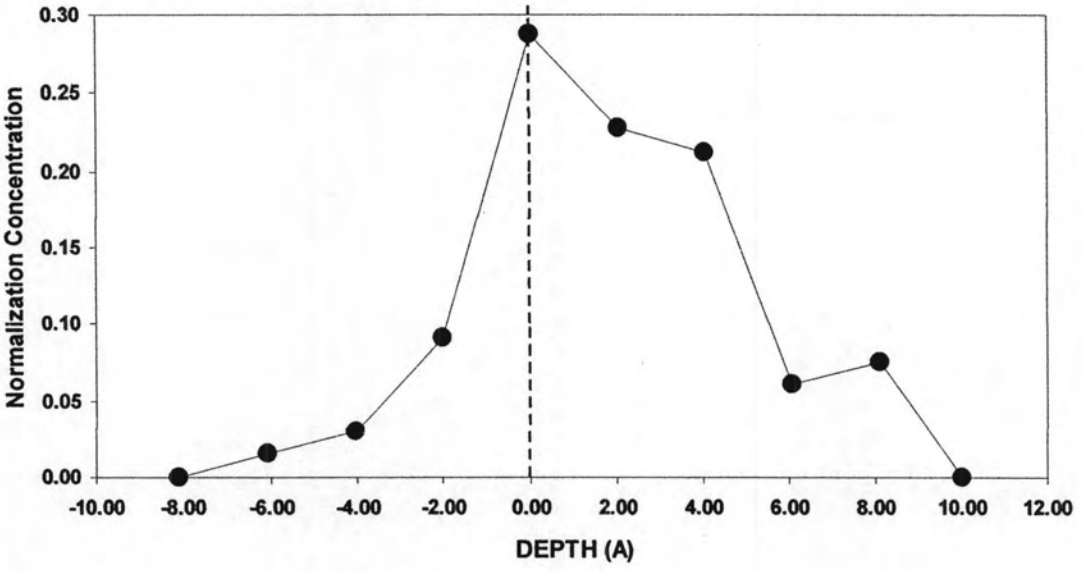

Fig. 4.33 the distribution of the 200eV coating ions
with Z = 78 in the SC target with Z = 26

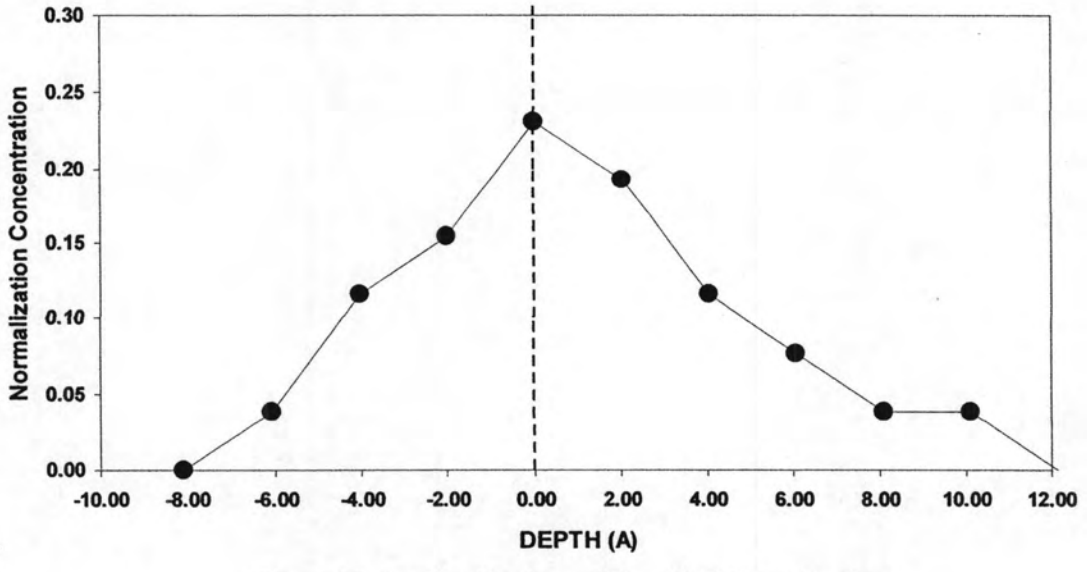

Fig. 4.34 the distribution of the 300eV coating ions
with Z = 78 in the SC target with Z = 26

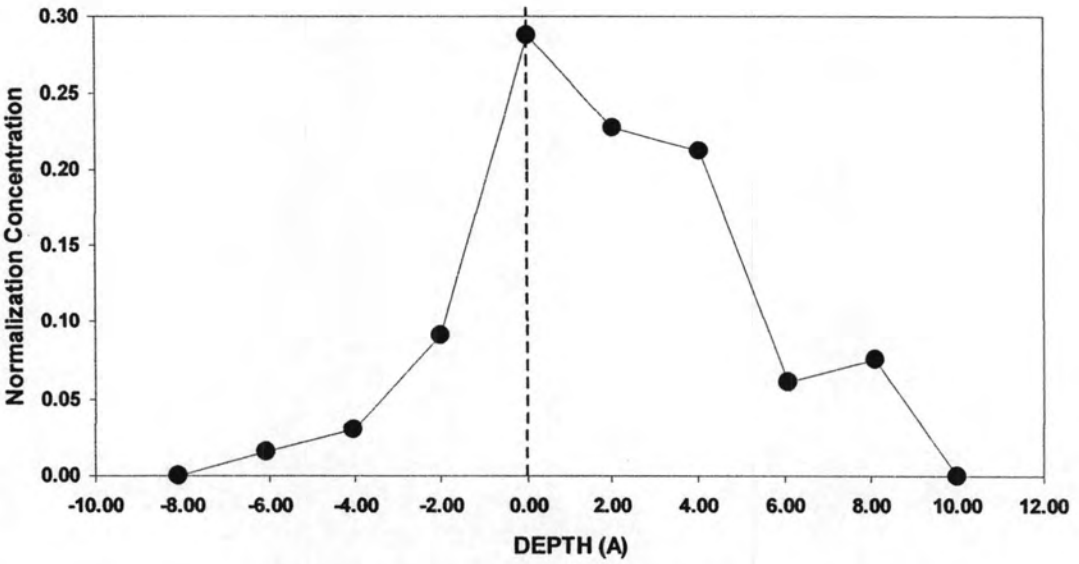

Fig. 4.35a the distribution of the 200eV coating ions
with Z = 78 in the SC target with Z = 26(random type 1)

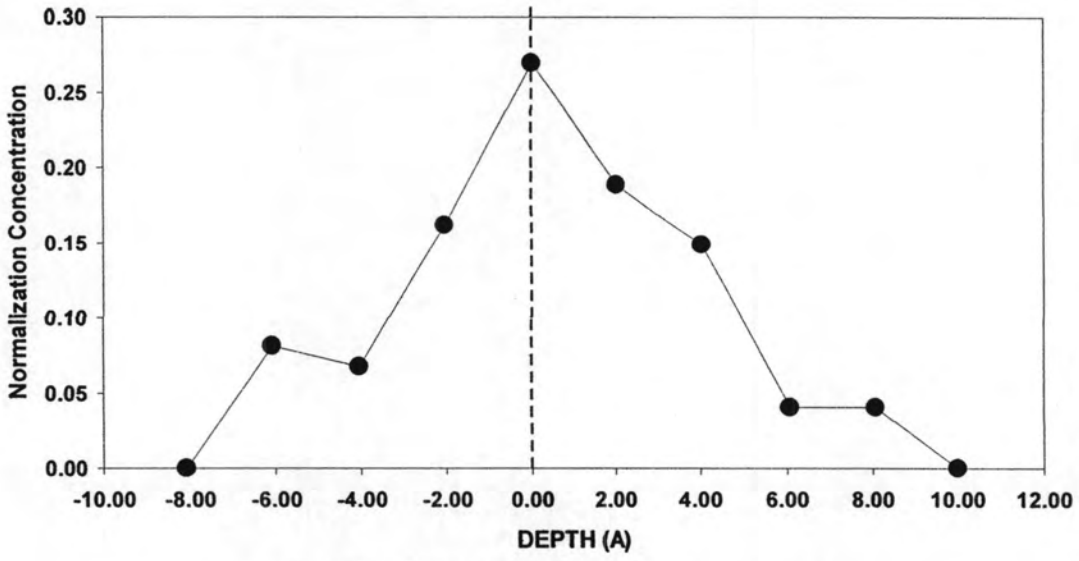

Fig. 4.35b the distribution of the 200eV coating ions
with Z = 78 in the SC target with Z = 26(random type 2)

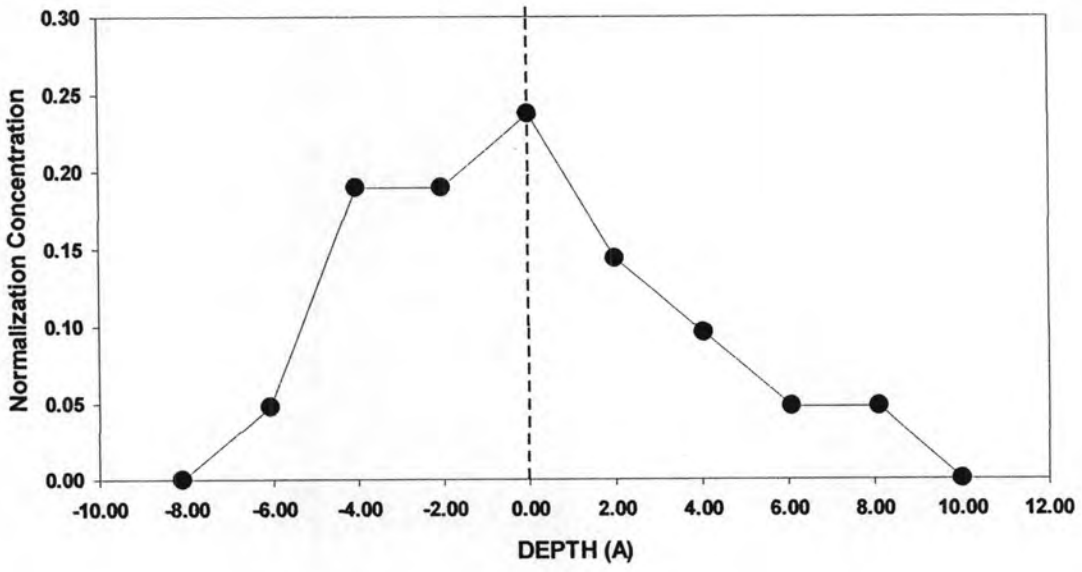

Fig. 4.35c the distribution of the 200eV coating ions
with Z = 78 in the SC target with Z = 26(random type 3)

Table 4.4 the properties of the coating layer

Energy (eV)	Generation Time (picoseconds)	Coating layer depth (A)	Ion density in coating layer (ion/m^3)
100	5.6212	5.5645	2.49394E+29
200	5.1184	9.7466	2.67154E+29
300	6.6549	9.9933	4.79698E+29

The ion intensity in the coating layer is high in case of the ion with high energy. The effect of the ion energy in the ion intensity show in table 4.4. The first reason for this effect comes from the heavy projectiles that have a small angular scattering. And the second reason cause by the more difference in the ion range of the low energy in the coating zone.